A birefringent polarization modulator: Application to phase measurement in conoscopic interference patterns

F. E. Veiras, M. T. Garea, and L. I. Perez

Articles you may be interested in

Enhanced performance of semiconductor optical amplifier at high direct modulation speed with birefringent fiber loop
AIP Advances **4**, 077107 (2014); 10.1063/1.4889869

Invited Review Article: Measurement uncertainty of linear phase-stepping algorithms
Rev. Sci. Instrum. **82**, 061101 (2011); 10.1063/1.3603452

Birefringence measurement in polarization-sensitive optical coherence tomography using differential-envelope detection method
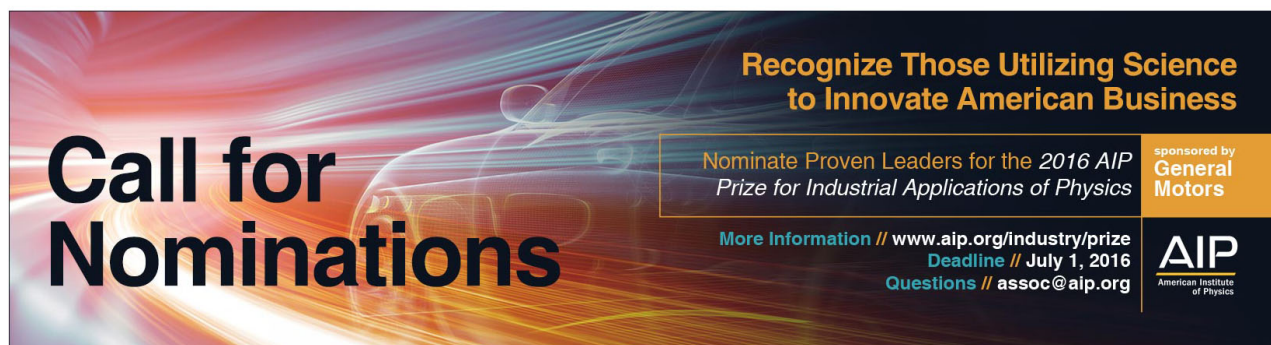Rev. Sci. Instrum. **81**, 053705 (2010); 10.1063/1.3418834

Phase Measurement and Interferometry in Fibre Optic Sensor Systems
AIP Conf. Proc. **1236**, 24 (2010); 10.1063/1.3426122

Note: Optical Rheometry Using a Rotary Polarization Modulator
J. Rheol. **33**, 761 (1989); 10.1122/1.550064

A birefringent polarization modulator: Application to phase measurement in conoscopic interference patterns

F. E. Veiras,[1,2,a)] M. T. Garea,[1] and L. I. Perez[1,3]

[1]*GLOmAe, Departamento de Física, Facultad de Ingeniería, Universidad de Buenos Aires,
Av. Paseo Colón 850, Ciudad Autónoma de Buenos Aires C1063ACV, Argentina*
[2]*CONICET, Av. Rivadavia 1917, Ciudad Autónoma de Buenos Aires C1033AAJ, Argentina*
[3]*INTECIN–CONICET, Av. Paseo Colón 850, Ciudad Autónoma de Buenos Aires C1063ACV, Argentina*

Conoscopic interferometry for crystal characterization is a very well-known technique with increasing applications in different fields of technology. The advantage of the scheme proposed here is the introduction of a polarization modulator that allows the recovery of the phase information contained in conoscopic interferograms. This represents a real advantage since the most relevant physical information of the sample under study is usually contained in the phase of the fringe pattern. Moreover, this technique works successfully even when there are no visible fringes. The setup employed is a simple conoscopic interferometer where the elements under study correspond to two birefringent crystal slabs and a commercial mica wave plate. It allows the crystals to be characterized and the wave plate retardance to be measured as a function of the angle of incidence. The modulator itself consists of a single tiltable crystal plate which, by means of phase shifting techniques, permits the recovery of a phase map for each sample. It is inexpensive and it can be easily calibrated, so it works with a wide range of phase shifting interferometry algorithms. We show that our scheme is easily adaptable to algorithms that require either a low or high amount of interferograms. *Published by AIP Publishing.* [http://dx.doi.org/10.1063/1.4947134]

I. INTRODUCTION

There are many methods for crystal characterization. Some of them are based on the interaction of the crystal samples with neutrons, X-rays, and electrons. For example, by using X-ray diffraction, Laue patterns can help determine the orientation of crystallographic axes.[1] There are also many properties that can be extracted from the crystals using electron diffraction techniques by means of Kikuchi patterns.[2] However, an optical examination of a crystal might yield useful information, which may prevent the use of a more detailed but expensive and time-consuming method.[3] Birefringent crystals have long been studied by means of conoscopic interference techniques.[4–9] Furthermore, conoscopic techniques have several applications like multipurpose rangefinders,[10] surface inspection,[11] differential interference contrast microscopy,[12] visualization of polarization properties of optical vortex beams,[13] and waveplate characterization.[14] Accordingly, conoscopic fringe patterns are theoretically described with different levels of approximation by means of the phase shift introduced between the beams that propagate through a crystal sample.[15–17] However, the analysis techniques for conoscopic interference patterns described in the bibliography are generally based on very simple methods such as fringe counting or isochromates visualization.

In this work, we present a simple birefringent phase shifter that acts as a polarization modulator and we apply it to phase measurement in conoscopic setups by means of phase shifting

interferometry (PSI). We propose a birefringent polarization modulator (BPM) that can be used as a phase shifter in interferometers where the input signal splits into two linear orthogonal polarizations. The experimental design can be generally adapted to different interferometers leading to a number of different applications. As an example, crystal characterization is the natural application of this modulator.

First, we briefly describe the experimental setup and the phase retrieval techniques that can be applied to conoscopic interferometry. Then, we explain the working principle of the BPM and its operation in a conoscopic interferometric scheme as a phase shifter for PSI. The proposed methodology is tested by means of experimental results and theoretical calculations. We analyze the operation of two different BPMs along with different PSI algorithms for the characterization of a quartz crystal and a commercial mica retarder.

II. EXPERIMENTAL SETUP

The conoscopic measurements are based on the interference between ordinary waves and extraordinary waves due to an optically anisotropic sample when it is illuminated by a cone of light (convergent or divergent). The proposed conoscopic setup is shown in Fig. 1, where the impinging laser beam is expanded and transmitted through the birefringent plate or device under test (DUT). Due to its simplicity and robustness, the preferable method to achieve this is grinding an interface before the crystal sample.[4–6,14,16] Some DUTs can have their first interface ground (at $x = 0$) but some samples can be severely damaged and a piece of ground glass must be interposed before the DUT. In order to simplify the analysis, we assume that the samples considered are uniform crystals.

a)Electronic mail: fveiras@fi.uba.ar. URL: www.fi.uba.ar/laboratorios/glomae.
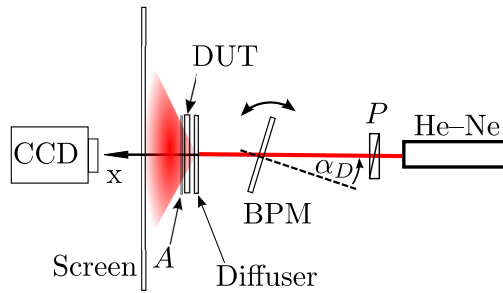
FIG. 1. Experimental conoscopic scheme (top view). From left to right: Camera (CCD), Screen, Analyzer (A), Device under test (DUT), Diffuser, Birefringent polarization modulator (BPM) mounted on a rotating stage at an angle α_D from the impinging beam, polarizer (P), laser (He–Ne).

Even in the most sophisticated experimental setups, the crystal sample is placed between the polarizer and the analyzer.[9] We keep the analyzer (A) and polarizer (P) in the scheme but add an extra birefringent plate (BPM) behind the polarizer to act as polarization modulator similar to the tilting stage proposed in Ref. 7. Due to its own birefringence, depending on the angle of incidence (α_D), this plate adds an extra phase shift between the interfering beams which can be controlled by means of a tilting stage. As a result, the fringe pattern moves according to the phase shift between components, allowing the identification of a number of properties.[18] However, we go further in order to obtain a phase map of the sample under study. This procedure not only allows us to clean the interferogram from unwanted illumination effects (removing almost everything but phase information) but also to characterize a crystal sample by means of the phase shift introduced. Thus, a comparison with theoretical calculations or an angular performance measurement of a polarization device, such as a retarder, can be accomplished.

A large numerical aperture (NA) cone of light is transmitted through the DUT in order to obtain as much phase information as possible. That is, the phase information is contained in a wide angle conoscopic interference pattern of high NA. However, the proposed experimental scheme allows us to work without high NA lenses since we collect the interferogram on a screen of coordinates (y, z) located behind the analyzer. Nevertheless, the basic scheme and the processing techniques can be fulfilled by means of an optical system with high NA lenses.

It should be noted that the complete interferometric setup corresponds to a common path interferometer and thus leads to a high level of immunity to ambient perturbations. For this experimental setup, the branches of the interferometer are superposed in space but only separated by their polarization.

In Sec. III, we present the phase retrieval problem associated to conoscopic interferometry and we explain how to extract the phase from the interferograms by means of PSI techniques assisted by a BPM.

III. INTERFEROMETRIC PHASE ESTIMATION

As reported in Refs. 4, 5, and 16–19, the interferograms corresponding to uniaxial crystals have a strong dependence on the direction of the optical axis, $\check{z}_3$ (given by θ, Fig. 2(a)).

The conoscopic interferograms show different phase distributions $\Delta\phi(y, z)$ which naturally lead to different ways of recovering the phase. In the case of a quartz plate with its optical axis at $\theta \approx 45°$ (Fig. 2(b)), the interferograms have a significant spatial frequency component.[17] Moreover, the phase recovery technique allowed by this frequency component is so simple that we benefit from it to develop a phase demodulator.[14] These interferograms can be easily processed by means of the Fourier transform method (FTM)[20] without the need of using the birefringent phase modulator. Each row of pixels from Fig. 2(b) can be processed separately using the Fourier transform and consequently filtering around the carrier frequency or directly by means of the Hilbert transform. The final phase map is therefore built by means of a 2-D phase unwrapping process that might be assisted by median smoothing.

The problem of phase retrieval arises in the case of more complicated interferograms, as in the case of hyperbolic fringe patterns (Fig. 2(c)). It gets even worse if there are no visible fringes: for example, in the case of thin mica wave plates (Fig. 2(d)). To overcome these limitations, we propose to employ a birefringent phase shifter that allows the introduction of phase shifts between the interfering beams and consequently the application of PSI algorithms.[21]

In general, PSI algorithms determine the unknown phase $\Delta\phi(y, z)$ over the pupil plane by calculating the arctangent of the ratio between two weighted summations (i.e., two linear combinations) of N phase shifted interferograms[22–24]

$$\Delta\phi(y, z) = \arctan\left[\frac{\sum_{i=1}^{N} n_i I_i(y, z)}{\sum_{i=1}^{N} d_i I_i(y, z)}\right], \qquad (1)$$

where n_i and d_i are the weights of the i-th recorded phase shifted interferogram $I_i(y, z)$ for the summation in the numerator and the denominator correspondingly.
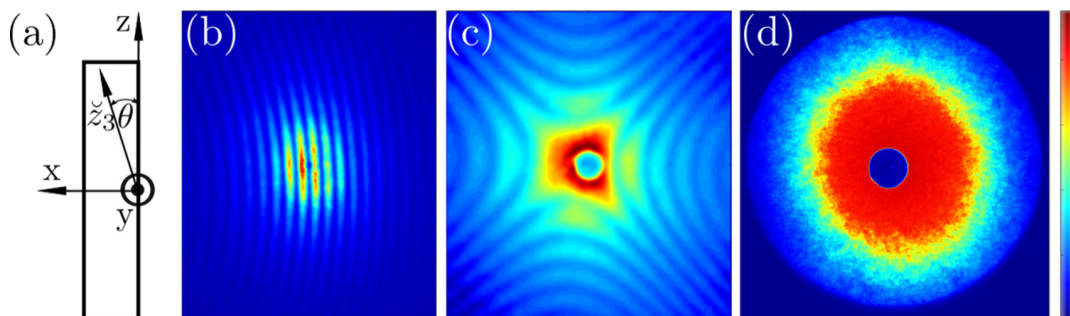

FIG. 2. (a) Detail of the DUT (e.g., uniaxial crystal). Conoscopic interferograms (plane (y,z), arbitrary units) obtained with different DUTs: 3 mm thick quartz plates (b) $\theta \approx 45°$ and (c) $\theta \approx 0°$, (d) commercial mica wave plate.

A. Phase shifting techniques with uniaxial crystal tilting plates

PSI techniques are based on the introduction of phase shifts by means of a phase shifter. For a polarization interferometer, we propose to use a birefringent polarization modulator (BPM) as a phase shifter, which consists of tilting a plane–parallel uniaxial crystal plate. The tilting of the birefringent plate is performed around the vertical axis of the optical setup by means of a rotating stage Newport RVS80CC (Fig. 1). The birefringent plate is fixed to the rotatory stage and its optical axis is adjusted perpendicularly to its rotation axis (vertical axis). This way, we obtain mode separation. The ordinary waves can be associated to s-polarized incident waves, and the extraordinary waves to the p-polarized ones. We adjust the polarizer P close to 45° from the horizontal plane in order to evenly split the incoming light into these modes. The phase shift between them can be varied by rotating the BPM to different angles. Accordingly, the polarization state after the BPM changes.

One of the BPMs we employ consists of a quartz crystal with its optical axis cut at $\theta \approx 45°$ from its interfaces. As the BPM rotates, the phase shift between these orthogonal modes varies according to[17,25]

$$\Delta\phi_{s-P}^{\theta=45°}(\alpha_D) \simeq \frac{2\pi H}{\lambda_v}\left[A + B\,\sin\alpha_D\right], \qquad (2)$$

where A and B remain constant for a given wavelength and are defined in Ref. 17. For small angles, the phase shift introduced varies linearly with the angle of incidence on the BPM, α_D. However, there are other crystals which, due to their phase shifting features, can be of interest to build a BPM.[17,25] For example, crystals with their optical axis at 90° from their interfaces are very attractive since there is no need for alignment due to their symmetry. The phase shift introduced depends on the angle of incidence according to

$$\Delta\phi_{s-P}^{\theta=90°}(\alpha_D) \simeq \frac{2\pi H}{\lambda_v}C_Z\,\sin^2\alpha_D, \qquad (3)$$

where C_Z remains constant for a given wavelength and is also defined in Ref. 17. It might be tempting to introduce absolute phase values instead of relative phase shifts since, according

to the above equation, $\Delta\phi_{s-p}(\alpha_D \to 0) \to 0$. However, in the proximities of the *isotropic point*, the effects of linear birefringence can be very low in comparison with other characteristics such as optical activity or chirality.[26,27]

In Eqs. (2) and (3), λ_v corresponds to the wavelength employed and H to the thickness of the BPM. In addition, A, B, and C_Z remain constant for a given wavelength and are defined in Ref. 17.

Both the BPM and the crystal under study are placed with their y principal axes parallel to the vertical axis. Thus, the BPM modifies the phase shift between the transmitted beams in the conoscopic setup. Consequently, the interference over the plane of detection can be written as

$$I(y, z, \Delta\phi_{s-P}) = a(y, z) + b(y, z)$$
$$\times \cos\left[\Delta\phi(y, z) + \Delta\phi_{s-P}(\alpha_D)\right], \qquad (4)$$

where $\Delta\phi(y, z)$ corresponds to the unknown phase information associated to the crystal under study. This allows the application of a wide range of PSI algorithms.

Unlike other birefringent phase shifters such as azimuthally rotated wave plates, the BPM proposed here allows deeper phase modulations that even exceed the 2π interval. There are many PSI algorithms that do not require an accurate control of the phase shifts introduced. However, this BPM can be easily calibrated, so it can be used with several algorithms that require different quantities of interferograms. In Sec. IV, we show experimental results obtained with different types of PSI techniques performed by different BPMs.

IV. EXPERIMENTAL RESULTS

A. Phase shifting interferometry without accurate control of the phase shift

First, we apply this technique by means of one of the BPMs, which consists of a plane parallel quartz plate with its optical axis perpendicular to its interfaces (Eq. (3)). The DUT is another 3 mm thick plane–parallel quartz plate with $\theta \approx 0°$. We interpose a ground interface very close to the first interface of the crystal plate, at a distance of (62 ± 5) mm from the screen. The size of the screen is (10.5 ± 0.1) cm
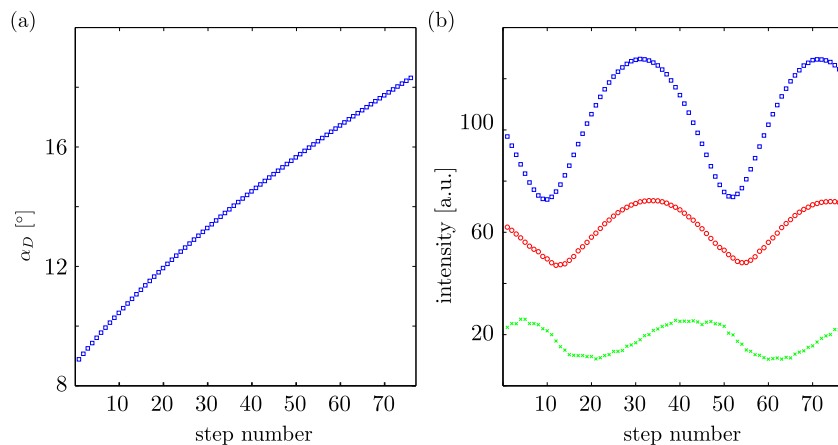

FIG. 3. (a) Angles of incidence α_D versus step number (75 steps). (b) Pixel intensity variation versus step number for three different pixels: $(300, 300)$ blue squares, $(400, 100)$ red circles, and $(30, 30)$ green crosses.
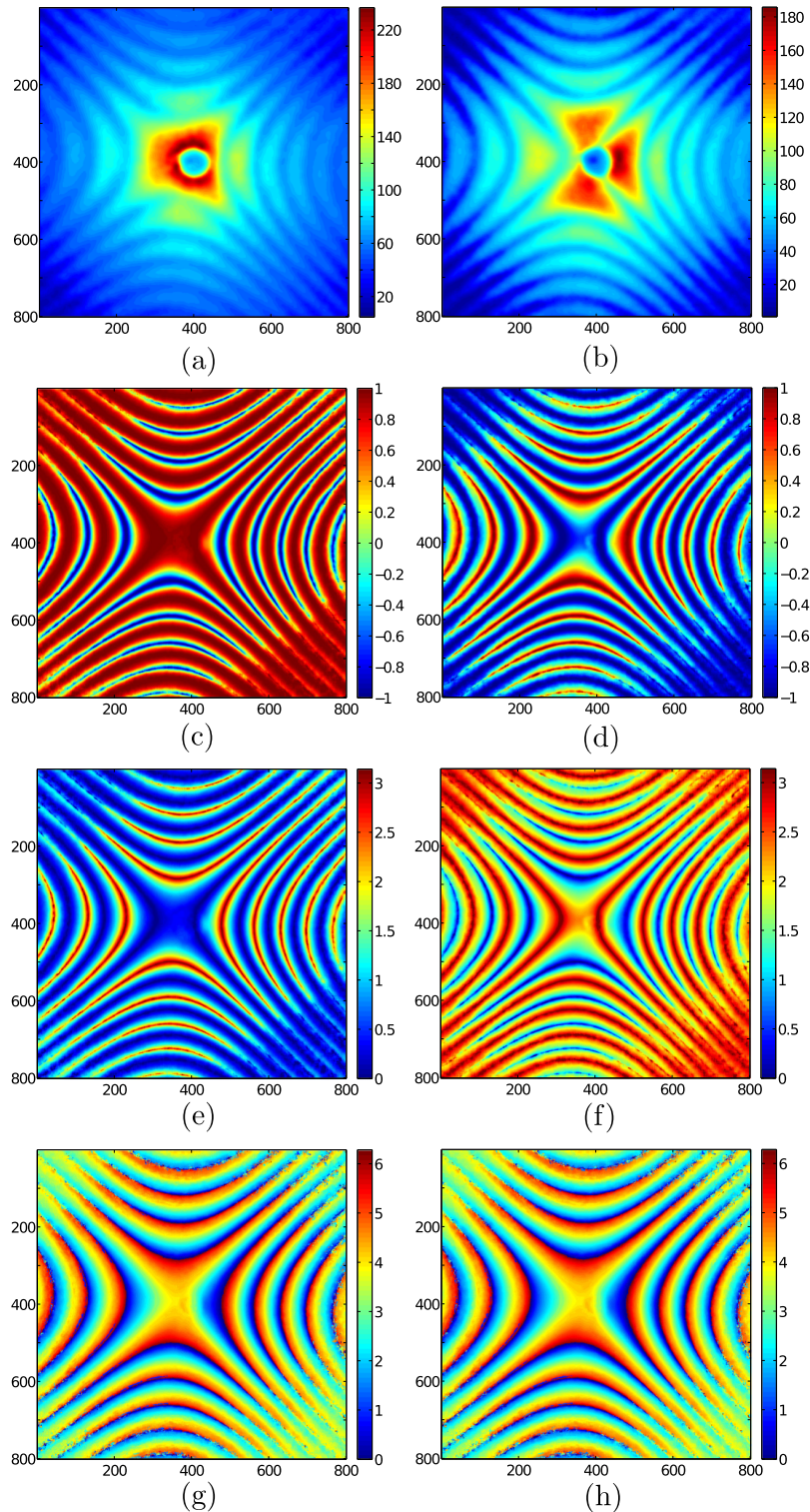
FIG. 4. Phase recovery sequence for uncalibrated phase shifts. DUT: 3 mm thick plane–parallel quartz plate with $\theta \approx 0°$. $\lambda_v = 632.8$ nm. Examples over the interferograms obtained in steps 39 and 59, respectively. Interferograms registered (arbitrary units between 0 and 255): (a) Step 39. The angle of incidence $\alpha_D = 14.53°$ on the BPM. (b) Step 59. The angle of incidence $\alpha_D = 16.74°$ on the BPM. (c) and (d) Cosine of the phase. (e) and (f) π modulus phase [rad]. (g) and (h) 2π modulus phase [rad].

and is discretized in an 800×800 pixel matrix. We vary the angle of incidence α_D on the BPM from $9°$ to $16°$ with a spacing between measurements, which allows us to obtain a fully sampled sinusoid (Fig. 3). The phase shift introduced, $\Delta\phi_{s-p}(\alpha_D)$, grows monotonically and the horizontally polarized wave is increasingly delayed (since $n_e > n_o$). This phase

shift introduced between these orthogonal components has a global impact on all of the pixels of the interferogram (Eq. (4)) and modifies the fringe pattern.[14,18]

We follow the procedure indicated in Ref. 28 in order to recover the phase map of the DUT. Unlike classical PSI algorithms, the one proposed there does not need the phase

shift step length as a parameter. Fig. 3(b) shows that there are more than forty samples for each period. Moreover, the mean phase step can be estimated by means of the signals of Fig. 3(b). Since the phase shift introduced is monotonic, the intensity over each pixel of coordinates (y,z) is approximately sinusoid (Fig. 3(b)) and allows the determination of $a(y,z)$ and $b(y,z)$ (Eq. (4)). Pixels belonging to the center of Figure 2(c), such as pixel $(300,300)$ (Fig. 3(b)), have a mean value $a(y,z)$ and an amplitude $b(y,z)$ higher than those in pixels from the periphery (e.g., pixel $(400,100)$). Distant pixels such as $(30,30)$ also indicate noticeable presence of noise.

The global impact of the phase shift $\Delta\phi_{s-p}(\alpha_D)$ introduced by the BPM over the interferogram (Eq. (4)) can be appreciated in Figs. 4(a) and 4(b). Those interferograms correspond to two different angles of incidence α_D on the BPM corresponding to steps 39 and 59, respectively.

We capture a sequence of 75 interferograms for a monotonically growing phase shift $\Delta\phi_{s-p}(\alpha_D)$ and apply the following procedure to them (Fig. 4). By means of the estimations of $a(y,z)$ and $b(y,z)$, and Eq. (4), we obtain the cosine of the phase $\Delta\phi(y,z) + \Delta\phi_{s-p}(\alpha_D)$ for each interferogram (Figs. 4(c) and 4(d)). Those matrices are $[-1,1]$ valued and by means of the arc cosine we recover the π modulus phase (Figs. 4(e) and 4(f)). Taking advantage of the monotonic phase shift introduced, it is possible to obtain the 2π modulus phase (Figs. 4(g) and 4(h)) and then unwrap the phase. In order to minimize the presence of noise (which is higher in the peripheral pixels), we apply median filters on the sine and cosine of the 2π modulus phase. We also restrict the phase map to a central area of 600×600 pixels

and run the unwrapping algorithms developed in Ref. 29 and available on Ref. 30. We take an arbitrary pixel for phase reference and average the unwrapped phase corresponding to 60 interferograms (Figs. 5(a) and 5(b)).

The results presented in Fig. 5 are comparable to those obtained with the formulas in Ref. 17 for the measured sizes and distances, with $\lambda = 632.8$ nm, $n_o = 1.54$, and $n_e = 1.55$ (Fig. 5(d)). The estimated value of θ corresponds to $-1.5°$ with a sensitivity of $0.1°$. Unlike the results in Ref. 31, the angle between the hyperbola asymptotes and the z axis for a quartz plane–parallel plate with θ close to zero coincides with that predicted in Ref. 17. Due to the complexity of the phase shift formulas for uniaxial crystals, a pixel by pixel fitting procedure would require a more accurate control of the experimental parameters in order to reduce experimental uncertainties (for example, dimensions or distance measurements). Consequently, a quantitative comparison between the interferograms of Figs. 5(c) and 5(d) such as the root mean square of the difference or the structural similarity index[32] would validate the model quantitatively.

In order to determine characteristic parameters such as θ or the principal refractive indices, different fitting procedures can be applied. The experimental setup presented here represents an advantage, since it enables to work directly with the phase information $\Delta\phi(y,z)$. However, this phase information itself corresponds to valuable information regarding the DUT, particularly about the phase shift that it is capable of introducing. This is a very important feature for the evaluation of phase retarders and the technique presented here is applied to a commercial wave plate (Fig. 2(e)).
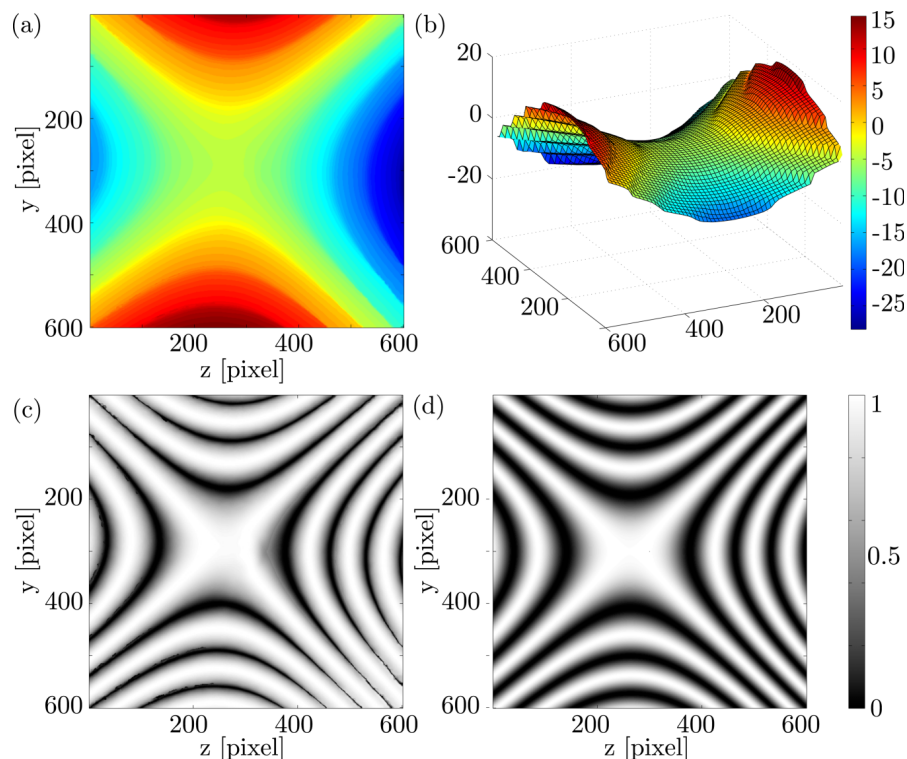

FIG. 5. DUT: 3 mm thick plane–parallel quartz plate with $\theta \approx 0°$. $\lambda_v = 632.8$ nm. Unwrapped phase map $\Delta\phi(y,z)$ [rad]: (a) (y,z) 2-D colormap and (b) 3-D representation. $I(y,z)$ Reconstructed interferogram [arbitrary units]: (c) Based on experimental data. (d) Theoretically generated interferogram for a 3 mm thick quartz plate $\theta = -1.5°$.

B. Classical phase shifting interferometry

In this experiment, the DUT is a commercial mica wave plate (Melles Griot 02WRM009 Mica Retarder Type, 1/4 WAVE 50 mm, K1788) which has a presumable slight angular dependence on the phase shift introduced. Accordingly, in Fig. 2(d) we can observe small phase variations across the conoscopic interferogram. In order to determine these phase variations, we first apply a 4-step PSI algorithm with a step size of $\pi/2$[33] by means of the $\theta \approx 45°$ BPM (Eq. (2)). It should be noted that a calibration of the BPM[14] or a self-calibrating algorithm is needed. The interferograms of Figs. 6(a)-6(d) have a relative phase shift of $\pi/2$ as indicated in Table I.

By means of these interferograms the phase can be recovered by

$$\Delta\phi(y,z) = \arctan\left[\frac{I_4(y,z) - I_2(y,z)}{I_1(y,z) - I_3(y,z)}\right]. \quad (5)$$

Figure 6(e) shows the angular dependence of the phase shift introduced by the wave plate. This figure shows a fluctuation around normal incidence that differs from the expected

TABLE I. Phase shifts introduced by the BPM $\theta \approx 45°$.

$I_i(y,z)$	α_D (deg)	$\Delta\phi_{s-p}(\alpha_D) - \Delta\phi_{s-p}(\alpha_D = 0°)$
$I_1(y,z)$	−0.8	−$\pi/2$
$I_2(y,z)$	0	0
$I_3(y,z)$	0.8	$\pi/2$
$I_4(y,z)$	1.6	π

smooth behavior (central zone in red). This is due to the deformation of the intensity signal $I(\Delta\phi_{s-p})$ for the pixels belonging to this region. Figure 6(f) shows the intensity variations for different pixels of the interferogram as $\Delta\phi_{s-p}$ is increased by means of the BPM. The blue squares correspond to the intensity for a pixel from the central zone which exhibits severe nonlinearities. In the case of peripheral pixels (red circles and green crosses) the intensity variations remain closer to sinusoids despite the higher levels of noise. A deeper study on the origin of these nonlinearities is still pending. However, it is known that PSI algorithms with fewer interferograms are
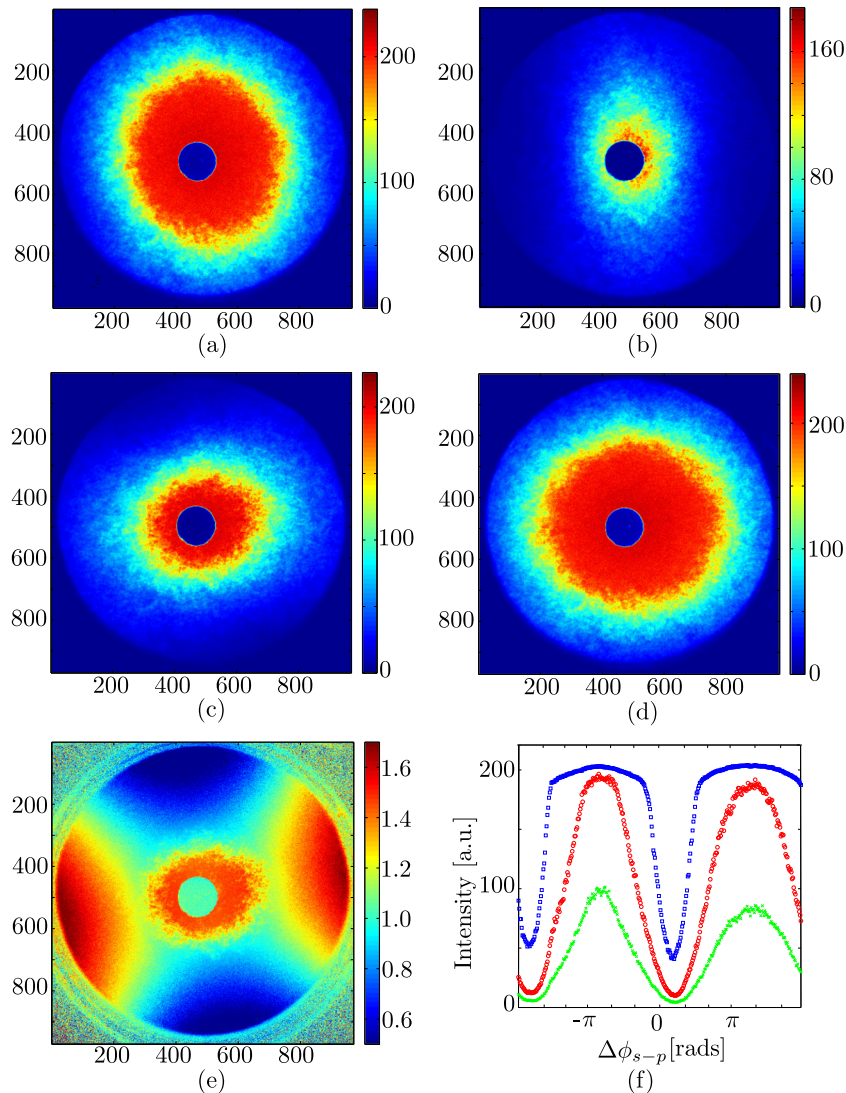

FIG. 6. DUT: Commercial mica wave plate $\lambda_v = 543.5$ nm. (a)–(d) Four registered interferograms $I_i(y,z)$ with relative phase shifts of $\pi/2$. (e) Phase recovered by means of the four-step PSI algorithm $\Delta\phi(y,z)$ [rad]. (f) Intensity variation as a function of the phase shift $\Delta\phi_{s-p}$ for three different pixels: $(600,500)$ blue squares, $(300,300)$ red circles, and $(230,230)$ green crosses.

more sensible to these nonlinearities as well as to phase shifter calibration errors. That is, the higher the number of interferograms in the algorithms, the more robust they get against different perturbations such as phase shifter errors or nonlinearities in the detection system. The properties of different PSI algorithms have been thoroughly studied.[34,35] Generally speaking, as we increase the number of interferograms, it is possible to make a selective filtering over $I(\Delta\phi_{s-p})$. This allows us to compensate for certain systematic and random errors, which can be analyzed by its Fourier representation. A complete and adequate review of these techniques is presented in Ref. 23. There, the authors identify the application of PSI

algorithms with the filtering process in the reciprocal space and subsequently analyze them according to their frequency representation. Accordingly, the weights of each interferogram (i.e., n_i and d_i in Eq. (1)) can be adjusted to cancel the higher order harmonics that do not follow the sinusoidal variation. Then, it is still possible to properly recover the phase information even with these distorted signals without modifying the experimental scheme.

There is a variety of PSI algorithms that require more interferograms in order to improve the recovered phase. We apply an 11-step PSI algorithm with a step size of $\pi/3$[35,36] by means of the $\theta \approx 45°$ BPM (Eq. (2))

$$\Delta\phi(y,z) = \arctan\left[\frac{\sqrt{3}(-I_0 - 2I_1 + 4I_3 + 5I_4 - 5I_6 - 4I_7 + 2I_9 + I_{10})}{I_0 - 2I_1 - 6I_2 - 4I_3 + 5I_4 + 12I_5 + 5I_6 - 4I_7 - 6I_8 - 2I_9 + I_{10}}\right], \tag{6}$$

where $I_i = I_i(y,z)$. By means of this algorithm, we cancel the harmonics of $I(\Delta\phi_{s-p})$ that affect the pixels in the central zone and recover the complete phase information over the region of interest (Fig. 7).

As can be seen in Figs. 6(a)–6(d), there are no distinguishable fringes. Accordingly, in Fig. 7 there are relatively small phase variations across the phase map. Since the phase does not exceed 2π, there is no need for phase unwrapping.

The results obtained give a measurement of the phase variations against the direction of incidence. The phase shift grows if the incidence is oblique over a plane which is approximately horizontal and diminishes over a vertical plane (Fig. 7). The measurements can be expressed as a function of the direction of incidence by considering that the distance from the ground plate to the screen is 5.8 cm and the pixel size is 0.054 mm. The maximum angle of incidence on the DUT is 24° approximately (i.e., a numerical aperture $NA \approx 0.4$). If the plane of incidence is the vertical plane, it is possible to reach a phase shift of 0.70 rad. Conversely, if the plane of incidence is horizontal, the phase shift introduced may reach a maximum difference of 0.56 rad regarding the phase shift for normal incidence. The phase recovered is referenced to an arbitrary constant and

for a complete characterization of the retarder performance it should be fixed to the phase shift for normal incidence.[14] The retarder is rather insensitive to the angle of incidence, since the phase shift variations between the central zone and the periphery do not exceed 0.70 rad. However, this difference might become relevant if working with highly divergent beams.

The procedure followed in Subsection IV A does not require a calibration of the phase step. Instead, in Subsection IV B, the phase step introduced by the BPM requires specific phase shift values. Thus, the phase step and the corresponding tilting angles (α_D) can be determined by means of the intensity signals of Fig. 6(f). However, this determination can also be performed with fewer measurements by means of a birefringent phase demodulator as the one described in Ref. 14.

The experimental results show that the conoscopic scheme in conjunction with the proposed BPM is suitable for crystal characterization and angular characterization of the retardance. In order to achieve this, we employ PSI algorithms with different complexities by means of this BPM. It allows us to work either with or without calibrated phase shifts. As we increase the number of steps, we are able to mitigate the effects of nonlinearities of the CCD. However, if the dynamic
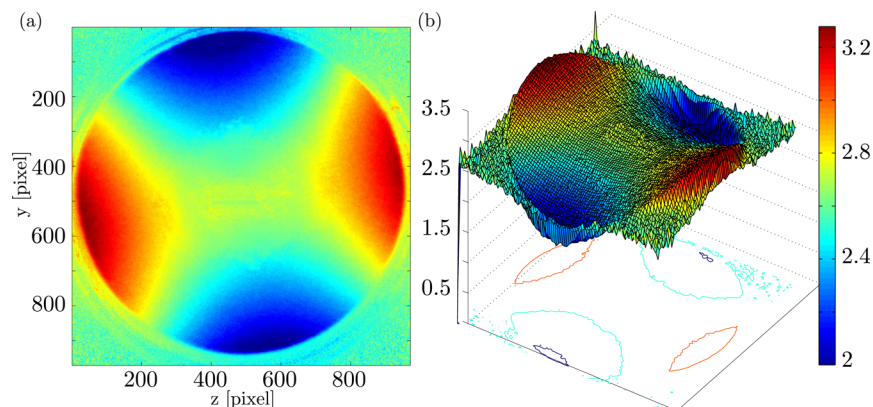

FIG. 7. DUT: Commercial mica wave plate $\lambda_v = 543.5$ nm. Phase recovered by means of the 11-step PSI algorithm $\Delta\phi(y,z)$ [rad]. (a) 2-D phase map. (b) 3-D representation.

range is restricted to a linear zone, algorithms with fewer interferograms can also be applied.

It would be desirable to estimate more characteristic parameters of the DUTs such as their thickness and their principal refractive indices as well as the different distances involved in the experiments. Due to the apparent complexity of the fitting problem, we have left the full characterization of crystal samples open for future analysis. Nevertheless, we believe that the methods proposed here are very useful for angular characterization of crystal samples and phase retarders.

V. CONCLUSIONS

We have shown the capabilities of a method based on PSI algorithms that is suitable for crystallographic studies and retardance measurement of polarization control devices. The methodology proposed here allows the extraction of the phase information contained in conoscopic interferograms with different phase distributions. Moreover, the experimental scheme and processing techniques can be easily implemented for optical crystallographic studies with relatively economical laboratory equipment.

There are still a number of further studies and improvements to carry on. In particular, those related to the influence of different experimental parameters on the recovered phase map. For example, the diffuser has proven to be a robust and reliable method to obtain a high NA beam which, combined with the rest of the experimental setup, is immune to vibrations. However, a complete study of capabilities and limitations of the experimental setup remains to be performed.

Consequently, this work sets the basis for future studies and developments. In addition, the presented BPM can also be employed as a phase shifter in different interferometric schemes. In this case, the base interferometer employed should have its arms separated by their polarization. For interferometers such as Michelson or Mach–Zehnder, the phase shift can be introduced by means of the BPM after the recombination of the reference and test beams (i.e., in a common path zone before detection). However, beam displacement due to the tilting of the plate should be taken into account or compensated for. The obtained results demonstrate the capabilities of the phase shifter, which is actually a polarization modulator.

ACKNOWLEDGMENTS

[1] T. Kikuchi, Rigaku J. **7**, 27 (1990).
[2] R. A. Schwarzer, Micron **28**, 249 (1997).
[3] M. Ladd and R. Palmer, "Examination of single crystals: Optical and x-ray diffraction practice," in *Structure Determination by X-Ray Crystallography: Analysis by X-Rays and Neutrons* (Springer US, Boston, MA, 2013), pp. 187–233.
[4] S. Jen and C. Hartmann, in *IEEE Proceedings of Ultrasonics Symposium* (IEEE, 1994), Vol. 1, pp. 397–401.
[5] P. Ayras, A. T. Friberg, M. Kaivola, and M. M. Salomaa, J. Appl. Phys. **82**, 4039 (1997).
[6] B. L. V. Horn and H. H. Winter, Appl. Opt. **40**, 2089 (2001).
[7] L. A. Pajdzik and A. M. Glazer, J. Appl. Crystallogr. **39**, 326 (2006).
[8] L. A. Pajdzik and A. M. Glazer, J. Appl. Crystallogr. **39**, 856 (2006).
[9] P. Wang, Opt. Lett. **37**, 4392 (2012).
[10] Y. Malet and G. Y. Sirat, J. Opt. **29**, 183 (1998).
[11] I. Álvarez, J. M. Enguita, M. Frade, J. Marina, and G. Ojea, Sensors **9**, 7021 (2009).
[12] C. Oh, S. O. Isikman, B. Khademhosseinieh, and A. Ozcan, Opt. Express **18**, 4717 (2010).
[13] M. M. Brundavanam, Y. Miyamoto, R. K. Singh, D. N. Naik, M. Takeda, and K. Nakagawa, Opt. Express **20**, 13573 (2012).
[14] F. E. Veiras, L. M. Riobó, C. L. Matteo, L. I. Perez, and M. T. Garea, Appl. Opt. **54**, 2326 (2015).
[15] M. Born and E. Wolf, *Principles of Optics*, 7th ed. (The Press Syndicate of the University of Cambridge, Cambridge, UK, 1999).
[16] M. C. Simon and M. T. Garea, Optik **87**, 95 (1991).
[17] F. E. Veiras, M. T. Garea, and L. I. Perez, Appl. Opt. **51**, 3081 (2012).
[18] O. Pikoul, J. Appl. Crystallogr. **43**, 955 (2010).
[19] M. Françon, in *Fundamental of Optics*, Encyclopedia of Physics Vol. XXIV, edited by S. Flugge (Springer-Verlag, Berlin, 1956).
[20] M. Takeda, H. Ina, and S. Kobayashi, J. Opt. Soc. Am. **72**, 156 (1982).
[21] P. Carré, Metrologia **2**, 13 (1966).
[22] K. Hibino, Opt. Rev. **6**, 529 (1999).
[23] B. V. Dorrío and J. L. Fernández, Meas. Sci. Technol. **10**, R33 (1999).
[24] Y. Surrel, in *Photomechanics*, Topics in Applied Physics Vol. 77, edited by P. Rastogi (Springer, Berlin, Heidelberg, 2000), pp. 55–102.
[25] F. E. Veiras, L. I. Perez, and M. T. Garea, Appl. Opt. **49**, 2769 (2010).
[26] Y. Vasylkiv, Y. A. Nastishin, and R. Vlokh, in *8-th International Conference on Laser and Fiber-Optical Networks Modeling*, *29 June–July 1* (IEEE, 2006), pp. 463–466.
[27] M. A. Geday and A. M. Glazer, J. Appl. Crystallogr. **35**, 185 (2002).
[28] Q. Hao, Q. Zhu, and Y. Hu, Opt. Lett. **34**, 1288 (2009).
[29] M. A. Herráez, D. R. Burton, M. J. Lalor, and M. A. Gdeisat, Appl. Opt. **41**, 7437 (2002).
[30] M. A. Gdeisat and M. A. Herráez, General Engineering Research Institute (GERI) at Liverpool John Moores University, Reino Unido, http://www.ljmu.ac.uk/geri/90207.htm, 2002.
[31] W.-Q. Zhang, Opt. Commun. **176**, 9 (2000).
[32] Z. Wang, A. Bovik, H. Sheikh, and E. Simoncelli, IEEE Trans. Image Process. **13**, 600 (2004).
[33] J. C. Wyant, Appl. Opt. **14**, 2622 (1975).
[34] P. de Groot, Appl. Opt. **34**, 4723 (1995).
[35] Y. Surrel, Appl. Opt. **36**, 271 (1997).
[36] K. Hibino, B. F. Oreb, D. I. Farrant, and K. G. Larkin, J. Opt. Soc. Am. A **12**, 761 (1995).